



## Full Length Article

# The adsorption characteristics of mercury species on single atom iron catalysts with different graphene-based substrates

Weijie Yang<sup>a</sup>, Zhengyang Gao<sup>a,\*</sup>, Xunlei Ding<sup>b</sup>, Gang Lv<sup>c</sup>, Weiping Yan<sup>a,\*</sup>

<sup>a</sup> School of Energy and Power Engineering, North China Electric Power University, Baoding 071003, China

<sup>b</sup> School of Mathematics and Physics, North China Electric Power University, Beijing 102206, China

<sup>c</sup> School of Mathematics and Physics, North China Electric Power University, Baoding 071003, China



## ARTICLE INFO

## Keywords:

Hg  
Adsorption  
Support effects  
Electronic structure  
Thermodynamic analysis

## ABSTRACT

Mercury (Hg) pollution caused by coal-fired power plants has raised global concerns, and it is imperative for developing a new low cost technology to control Hg emissions. Single atom iron catalyst with graphene-based substrates (Fe/GS) which has high catalytic activity and high selectivity is a promising material for removal of mercury pollution. The adsorption characteristics of mercury species on single atom iron catalysts with different graphene-based substrates were investigated systematically using first-principles calculation. It is found that the support effects of graphene-based substrates have a significant influence on adsorption characteristic of mercury species, and the support effects can be well understood through electronic structure analysis. Fermi softness is a good descriptor for adsorption activity of Fe/GS which can be an indicator for design and optimization of new materials. Fe/GS may be a new material for removal of Hg<sup>0</sup> pollutant, and the temperature has an inhibitory effect on mercury species adsorption. Furthermore, the findings can provide a novel perspective for adsorption and oxidation of Hg and lay a foundation for the further study of graphene-based support effects in single atom catalysts.

## 1. Introduction

Mercury (Hg), as one of the most hazardous trace elements, has caused worldwide concern for its volatility, persistence, and bioaccumulation in the environment. Coal-fired power plants have been identified as the main source of anthropogenic mercury pollution. In coal-fired flue gas, Hg exists mainly in three different forms: elemental mercury (Hg<sup>0</sup>), gaseous oxidized mercury (Hg<sup>2+</sup>), and particulate-bound mercury (Hg<sup>p</sup>) [1]. Hg<sup>p</sup> can be collected by electrostatic precipitators and fabric filters, and highly water-soluble Hg<sup>2+</sup> can be effectively captured by wet flue gas desulfurization. However, Hg<sup>0</sup> is difficult to remove by existing air pollution control devices due to its highly volatile and low solubility in water [2–4]. Therefore, the adsorbing Hg<sup>0</sup> to generate Hg<sup>p</sup> and oxidizing Hg<sup>0</sup> to convert Hg<sup>2+</sup> are effective ways to control mercury pollution from coal-fired power plants.

Due to the high toxicity and stringent regulation of Hg, various adsorbents and catalysts for controlling Hg emissions, including modified activated carbon [5–7], metal [8,9], metal oxides [10–12], kaolinite [13] and metal-organic framework [14] have been investigated. Unfortunately, there are many hindrances to apply these adsorbents

and catalysts widely in practical operation owing to its high cost and low efficiency [15]. Therefore, it is imperative globally for developing a new low cost technology to control Hg emissions from coal-fired power plants.

Recently, single atom catalysts (SACs) have attracted increasing attention in the field of heterogeneous catalysis owing to their high catalytic activity and high selectivity. As a type of novel heterogeneous catalyst, SACs promise to become a bridge between homogeneous and heterogeneous catalysis and show super catalytic activity in many industrial catalytic reactions [16–20]. Graphene is an excellent support for SACs because of its large specific surface area and unique physical and chemical properties [21]. SACs which are synthesized by embedding transition metal atoms in graphene-based substrates (TM/GS) can further reduce the cost of catalysts, and TM/GS have been widely investigated in many research field, such as CO oxidation [22–24], O<sub>2</sub> activation [25,26], CO<sub>2</sub> reduction [27], hydrogen evolution reaction [28] and oxygen evolution reaction [29,30]. Although TM/GS have been successfully applied to many industrial reactions, its application field remains to be further widened. Applying TM/GS to remove mercury pollution from coal-fired power plants is worth exploring, but there is limited investigations on the removal of Hg<sup>0</sup> through TM/GS.

\* Corresponding authors.

E-mail addresses: [gaozhyan@163.com](mailto:gaozhyan@163.com) (Z. Gao), [yanweiping@263.net](mailto:yanweiping@263.net) (W. Yan).

For the feasibility of TM/GS on the removal of  $\text{Hg}^0$ , there are many studies about controlling Hg emissions through carbonaceous materials modified by metal which proves that applying TM/GS to remove mercury pollution is advisable [31–34]. Fan et al. applied Cu-impregnated activated carbon to remove  $\text{Hg}^0$ , and concluded that the removal efficiency of  $\text{Hg}^0$  can reach 71% and the active sites are mainly the copper on carbonaceous surface [31]. Teresa Izquierdo et al. investigated the performance of carbonaceous materials supported Au nanoparticles for  $\text{Hg}^0$  removal in a fixed bed and found that the removal efficiency of  $\text{Hg}^0$  can reach 89% [33]. They also emphasized that the size of Au nanoparticle has significance influence on the removal efficiency of  $\text{Hg}^0$ , and the smaller the size of the nanoparticles, the higher the removal efficiency of  $\text{Hg}^0$  [33]. Therefore, it is quite plausible that carbonaceous materials supported Au nanoparticles can turn into SACs when the size of Au nanoparticles further decrease to single Au atom. Furthermore, Fan et al. investigated the adsorption of mercury species and catalytic oxidation of  $\text{Hg}^0$  on graphene-based materials modified by transition metal atoms and concluded that graphene-based material modified by Fe atom is a favorable heterogeneous catalyst for  $\text{Hg}^0$  oxidation because the oxidation energy barrier of  $\text{Hg}^0$  is the lowest (0.437 eV) [32]. However, the support effects of graphene-based substrates on the adsorption and catalytic oxidation of  $\text{Hg}^0$  was not considered in the research of Fan [32]. As supported catalysts, the support effects of SACs have significant influences on the performance of catalysts [35–38], which is helpful to understand the structure-activity relationship of SACs and design high efficiency catalyst.

In order to fill this gap, the adsorption characteristics of mercury species on single atom iron catalysts with different graphene-based substrates were comprehensively investigated using first-principles calculation. According to the previous researches [32,39], Fe/GS should be a promising catalyst for the removal of  $\text{Hg}^0$ . Therefore, we further investigate the adsorption characteristics of mercury species under different substrates based on Fe/GS so as to design for high activity catalysts and explore the support effects in SACs. Taking into account the catalyst preparation in practical, vacancy defects and nitrogen doping are common and accessible modification methods, four kinds of graphene-based substrates were constructed through vacancy defects and nitrogen doping to systematically study the adsorption characteristics of mercury species under different graphene-based substrates.

In this work, firstly, four different geometric structures of Fe/GS were optimized and key parameters such as bond length, charge and binding energy were discussed. Secondly, the adsorption characteristic of  $\text{Hg}^0$ , HgCl and  $\text{HgCl}_2$  were investigated respectively. The density of states analysis were performed to study the difference of  $\text{Hg}^0$  on Fe/GS, the potential energy diagrams for different pathways of HgCl and  $\text{HgCl}_2$  on Fe/GS were discussed to investigate the adsorption and desorption of HgCl and  $\text{HgCl}_2$  on Fe/GS. Thirdly, the *d* band center and Fermi softness analysis were conducted to reveal the support effects of graphene-based substrates on mercury species adsorption. Lastly, the thermodynamic analysis was carried out to investigate the effect of temperature on the adsorption characteristic of mercury species on Fe/GS. We hope this work can not only broaden the application field of SACs to promote the efficiency of  $\text{Hg}^0$  removal, but also lay a foundation for the further study of graphene-based support effects in single atom catalysts.

## 2. Calculation method

All calculations were performed with the first-principles method by the Vienna ab initio simulation package (VASP) with a projector augmented wave (PAW) method [40–42]. The generalized gradient approximation (GGA) with the Perdew-Burke-Ernzerhof (PBE) functional was adopted to treat the exchange correlation interactions [43]. The spin polarization was taken into account to obtain accurate ground-state energy [44]. According to the previous study, the adsorption of

$\text{Hg}^0$  on solid surface may be physical adsorption [45,46], the DFT-D3 method [47,48] was used to include the Van Der Waals interaction. Consistent with previous research models [49–51], a  $4 \times 4$  supercell of graphene was built as catalyst supports and the vacuum layer was set to 15 Å to avoid the interaction among mirror images [49,52].

Through the convergence test, the kinetic energy cutoff for the plane-wave basis set was chosen as 500 eV (as shown in Fig. S1 of supporting information). Gaussian smearing with a width of  $\sigma = 0.05$  eV was adopted for the occupation of the electronic levels [53]. For structure optimization, the positions of all atoms were allowed to fully relax with the conjugate gradient method until the maximum force on any atom was less than 0.02 eV/Å. Considering the computational time and accuracy, the Brillouin zone was sampled with a  $7 \times 7 \times 1$   $\Gamma$ -centered k-point grid for structure optimization calculation, and k-point grid selection was tested until energy change was less than 10 meV/atom (as shown in Fig. S1 of supporting information). While a  $15 \times 15 \times 1$   $\Gamma$ -centered k-point grid was used to calculate energy and density of states (DOS). Additionally, the convergence precision of total energy between two self-consistent steps was taken to be  $10^{-5}$  eV for structure optimization and DOS calculation.

The binding energy ( $E_b$ ) between Fe adatom and graphene-based substrates was defined as  $E_b = E_{\text{Fe/GS}} - E_{\text{sub}} - E_{\text{Fe}}$ , where  $E_{\text{Fe/GS}}$ ,  $E_{\text{sub}}$  and  $E_{\text{Fe}}$  are the total energy of Fe/GS, graphene-based substrates and Fe atom, respectively. The adsorption energies ( $E_{\text{ads}}$ ) of mercury species ( $\text{Hg}^0$ , HgCl and  $\text{HgCl}_2$ ) on Fe/GS were calculated to describe the interaction strength between mercury species and Fe/GS. The adsorption energies of  $\text{Hg}^0$ , HgCl and  $\text{HgCl}_2$  can be calculated according to  $E_{\text{ads}} = E_{\text{Hg-Fe/GS}} - E_{\text{Hg}} - E_{\text{Fe/GS}}$ , where  $E_{\text{Hg-Fe/GS}}$ ,  $E_{\text{Hg}}$  and  $E_{\text{Fe/GS}}$  are the total energy of adsorption systems, mercury species and Fe/GS, respectively. According to the calculation formula, a negative  $E_{\text{ads}}$  or  $E_b$  value represents a stable adsorption interaction, and a higher negative value of  $E_{\text{ads}}$  or  $E_b$  corresponds to a stronger adsorption [45]. Frequency calculation was performed to confirm the accuracy of equilibrium structures and to acquire zero point energy correction. There was no imaginary frequency in equilibrium structures. In detail, the vibrational frequencies were obtained from numerical Hessian calculations with finite displacements of  $\pm 0.02$  Å [54]. The energies of isolated Fe atom and mercury species ( $\text{Hg}^0$ , HgCl and  $\text{HgCl}_2$ ) were calculated in a large cell of  $9.84 \text{ \AA} \times 9.84 \text{ \AA} \times 15 \text{ \AA}$  with only  $\Gamma$  point. In addition, the binding energy and adsorption energy were calculated through zero point energy correction. Furthermore, Bader charge was calculated to quantitatively analyze the relevant electron transfer [55].

## 3. Results and discussion

### 3.1. Catalyst model

Taking into account the catalyst preparation in practical, vacancy defects and nitrogen doping are common and accessible modification method, four kinds of graphene-based substrates were constructed through vacancy defects and nitrogen doping to investigate the adsorption characteristic and support effects of graphene-based substrates. The optimized geometric structures of Fe/GS are shown in Fig. 1, and the corresponding bond length of C–Fe or N–Fe, adsorption height of Fe atom, charge of Fe atom, and binding energy are summarized in Table 1. In detail, the distance between Fe atom and graphene-based substrates plane was defined as the adsorption height of Fe atom. From Fig. 1, the adsorption height of Fe atom decreases gradually from (a) to (d), and the Fe atom almost locates in the graphene plane in Fe/DV-N4. From Table 1, the charge of Fe atom increases gradually from (a) to (d), and the charge of Fe atom in Fe/DV-N4 is biggest with a value of 1.081 e. Taking into account the stability of SACs, the cohesive energy of Fe bulk in experiment was selected as a reference to discuss it. The value of cohesive energy is 4.28 eV [56] which is smaller than the binding energies of Fe/GS, suggesting that Fe/GS should have high stability. In addition, the calculated results in this work correspond well

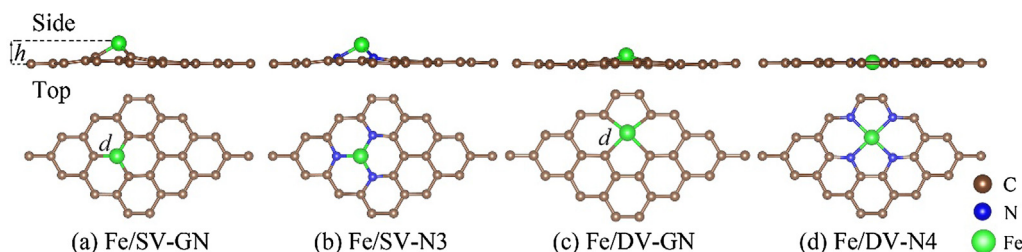


Fig. 1. The geometric structures of Fe/GS.

Table 1

The bond length of C–Fe or N–Fe ( $d$ , Å), adsorption height of Fe atom ( $h$ , Å), charge of Fe atom ( $q$ , e) and binding energy ( $E_b$ , eV) for Fe/GS.

Fe/GS	$d$ (Å)	$h$ (Å)	$q$ (e)	$E_b$ (eV)
Fe/SV-GN	1.762	1.345 (1.36 [57])	+0.687	−7.154 (−7.28 [23])
Fe/SV-N3	1.780	1.230	+0.889	−4.406
Fe/DV-GN	1.862	0.660 (0.67 [57])	+0.895	−6.123 (−6.47 [23])
Fe/DV-N4	1.887	0.053 (0.03 [58])	+1.081	−7.129 (−7.07 [59])

with the previous results, which can further guarantee the rationality and validity of this work [23,57–59].

### 3.2. Adsorption of mercury species

#### 3.2.1. $Hg^0$ adsorption

The stable adsorption configurations of  $Hg^0$  on Fe/GS are shown in Fig. 2. In previous study [39], the adsorption height of Fe atom will have an obvious variation in gas adsorption process, and there may be a negative relationship between uplift height of Fe atom ( $\Delta h$ ) and adsorption energy. In detail, a positive value of  $\Delta h$  means that the adsorption height of Fe atom increases. In addition, the adsorption process is usually accompanied by charge transfer, so the charge variations of Fe, Hg and substrates before and after adsorption process ( $\Delta q$ , e) were calculated, as shown in Table 2. In detail, a positive value of  $\Delta q$  means gaining electron.

From Fig. 2, Fe atom is the adsorption site of  $Hg^0$  on Fe/GS, which is same to the previous researches [32,60,61]. Different from previous study [39], there is no obvious relationship between the uplift height of Fe atom and adsorption energy. The bond length of Fe–Hg obviously varies on different Fe/GS, and there is a negative relationship between bond length of Fe–Hg and adsorption energy. The  $E_{ads}$  of  $Hg^0$  on Fe/SV-N3 is the biggest (−0.805 eV) with the smallest bond length of Fe–Hg (2.619 Å), suggesting that the adsorption of  $Hg^0$  on Fe/SV-N3 is chemisorption. Compared with other researches, the  $E_{ads}$  of  $Hg^0$  on Cu (1 1 1) [31], Au (1 1 1) [8] and CaO (0 0 1) [62] are −0.49, −0.42 and −0.24 eV respectively, which are all smaller than the  $E_{ads}$  of  $Hg^0$  on Fe/SV-N3, indicating that Fe/SV-N3 has higher adsorption activity for  $Hg^0$  than traditional materials.

From Table 2, the difference of adsorption energy between different Fe/GS is obvious, which suggests that the effect of graphene-based substrates on adsorption activity of SACs is significant. In detail, the value of  $E_{ads}$  on Fe/DV-N4 is positive which suggests that the adsorption of  $Hg^0$  on Fe/DV-N4 is unstable, and the adsorption of  $Hg^0$  on Fe/SV-GN and Fe/DV-GN is physisorption. The adsorption energy of  $Hg^0$  on Fe/SV-GN is −0.438 eV which is similar to the calculated results of Fan

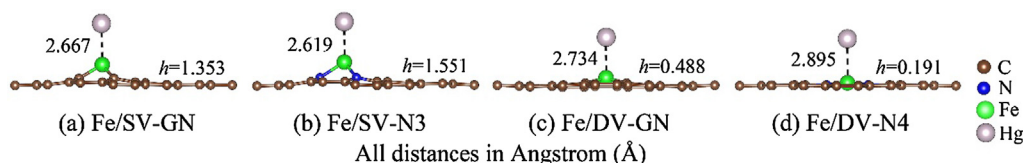


Fig. 2. The adsorption configurations of  $Hg^0$  on Fe/GS.

Table 2

The uplift height of Fe atom ( $\Delta h$ , Å) charge variation ( $\Delta q$ , e) and adsorption energy ( $E_{ads}$ , eV) for  $Hg^0$  adsorption system.

Fe/GS	$\Delta h$ (Å)	$\Delta q_{Hg}$ (e)	$\Delta q_{Fe}$ (e)	$\Delta q_{sub}$ (e)	$E_{ads}$ (eV)
Fe/SV-GN	0.008	−0.019	0.003	0.016	−0.438
Fe/SV-N3	0.312	0.052	0.007	−0.061	−0.805
Fe/DV-GN	−0.026	−0.021	0.012	0.007	−0.386
Fe/DV-N4	0.140	−0.006	0.091	−0.079	0.298

(−0.418 eV) [32], indicating the calculated results of this work is reliable. Different from Fe/SV-GN and Fe/DV-GN, the charge variation of  $Hg^0$  in Fe/SV-N3 is positive and the direction of electron transfer is from graphene-based substrates to  $Hg^0$ . Among the process of electron transfer, the Fe atom in Fe/SV-N3 act as bridge of electron transfer. The different electron transfer may be caused by the different adsorption interaction mechanism between chemisorption and physisorption.

In order to obtain the binding mechanism of  $Hg^0$  on Fe/GS and explain the difference of  $E_{ads}$  under different Fe/GS, the projected density of states (PDOS) was calculated to provide a further insight. The density of states (DOS) of a system describes the number of states per interval of energy at each energy level that are available to be occupied by electrons, and the PDOS examines the contribution from each energy band to a given atomic orbital [46,63]. The atom states shift down to lower energy states means a bonding between atoms, and greater hybridization of states leads to a stronger bond [32]. The PDOS of  $Hg^0$  and Fe atom under different Fe/GS were plotted in Figs. 3–6.

In Fig. 3 to Fig. 6, the  $s$ ,  $p$  and  $d$  orbital of  $Hg^0$  and Fe atom have been plotted, PDOS of  $Hg^0$  and Fe atom before and after adsorption are plotted in red solid line and blue dashed line. Before the adsorption of  $Hg^0$ , the  $s$  sharp peaks of  $s$ ,  $p$  and  $d$  states are −0.1, 5.7 and −3.1 eV which are well consistent with previous studies [46,62,63]. After the adsorption of  $Hg^0$  on Fe/GS, the  $s$ ,  $p$  and  $d$  states of  $Hg^0$  are all shift down to a lower energy states, indicating that there is an interaction between  $Hg^0$  and Fe/GS. Moreover, the shift distances of  $s$  and  $d$  states are proportional to adsorption energies of  $Hg^0$  on Fe/GS. In detail, the shift distance of occupied states in Fe/SV-N3 is biggest, and the adsorption of  $Hg^0$  on Fe/SV-N3 is also the biggest at the same time.

According to the frontier molecular orbital theory [64,65], the  $d$  states of metal atom in TM/GS play an important role in adsorption and reaction, so the  $d$  states variation of metal atom in adsorption process should be focused on. There is no obvious broadened in  $d$  states variation of Fe atom in the adsorption of  $Hg^0$  on Fe/SV-GN, Fe/DV-GN and Fe/DV-N4, implying that the bonding interaction between Hg and Fe atoms are weak. In addition, the PDOS analysis results of Fe/SV-GN are in agreement with the relevant research of Fan [32]. It is noteworthy,

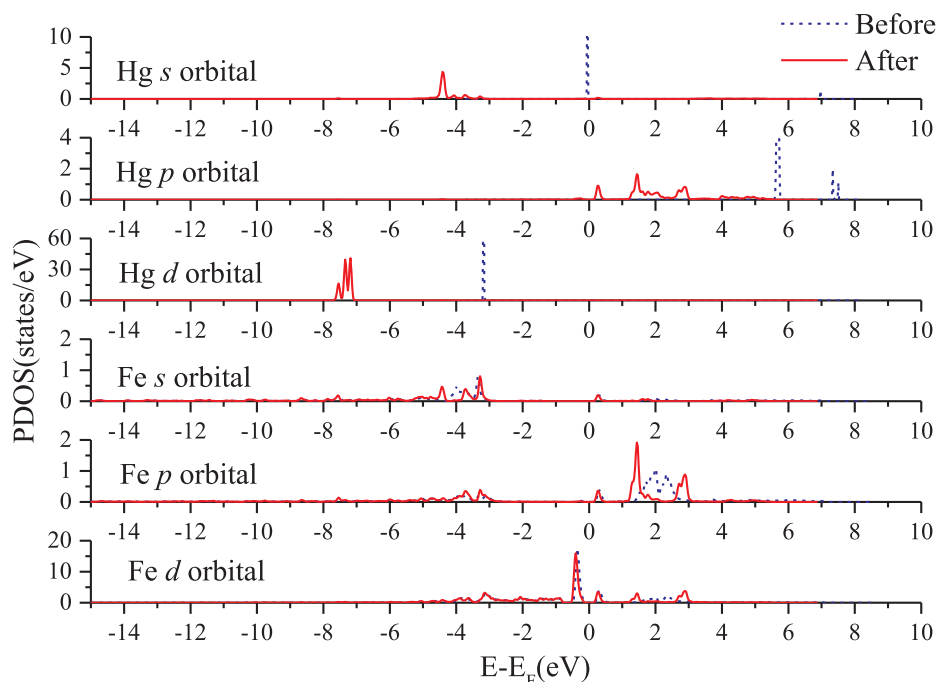


Fig. 3. The projected density of states diagrams of  $\text{Hg}^0$  and Fe atom on Fe/SV-GN.

there is an obvious broadened of Hg *d* states, which can be a good indication of strong interaction between Fe and Hg in Fe/SV-N3. Furthermore, based on the performance of  $\text{Hg}^0$  adsorption on different Fe/GS, we can conclude that the support effects of graphene-based substrates is one of the key factors that affect the adsorption activity of Fe/GS and the adsorption activity of Fe/GS can be significantly improved through doping nitrogen atoms.

### 3.2.2. HgCl adsorption

The stable adsorption configurations of HgCl on Fe/GS are shown in Fig. 7, and corresponding key parameters of adsorption process are

summarized in Table 3 and Table 4. In Fig. 7, there are two adsorption models, molecule and dissociation adsorption. In molecule adsorption model, the bond lengths of Hg–Cl are all slightly elongated compared to HgCl molecule (2.23 Å) [66], indicating that there is a bonding interaction between HgCl molecule and Fe/GS. In dissociation adsorption model, the bond lengths of Hg–Cl all exceed 3 Å, which suggests that there is no chemical interaction between Hg and Cl atoms. From Table 3 and Table 4, the  $E_{\text{ads}}$  of HgCl on Fe/GS is much higher than  $E_{\text{ads}}$  of  $\text{Hg}^0$  on Fe/GS, and the interaction between HgCl and Fe/GS belongs to chemisorption. Consistent with the adsorption of  $\text{Hg}^0$  on Fe/GS, the adsorption energies of HgCl on Fe/SV-N3 in two adsorption model are

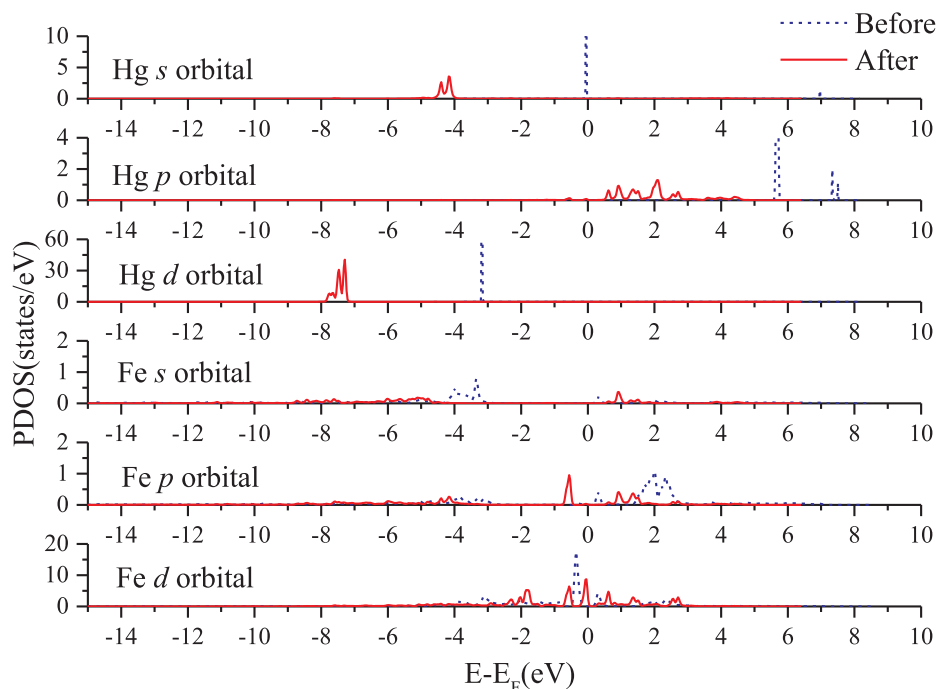


Fig. 4. The projected density of states diagrams of  $\text{Hg}^0$  and Fe atom on Fe/SV-N3.

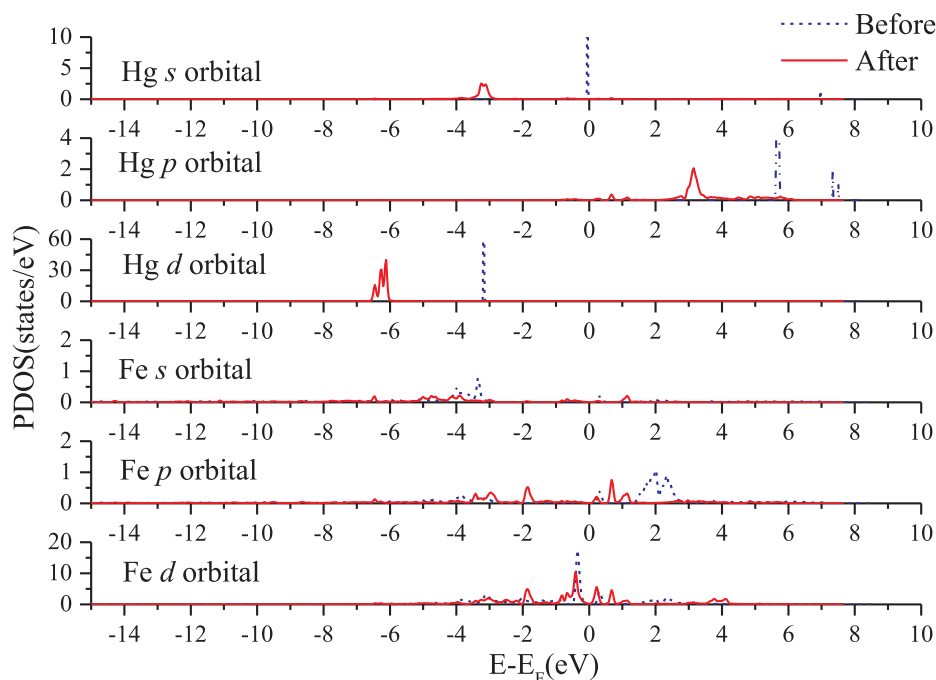


Fig. 5. The projected density of states diagrams of  $\text{Hg}^0$  and Fe atom on Fe/DV-GN.

all biggest, which confirms the high adsorption activity of Fe/SV-N3 for HgCl. Moreover, combined with adsorption energy and bond length, we can conclude that the longer the bond length of Hg–Cl is, the greater the adsorption energy of HgCl on Fe/GS is. It is worth noting that the charge variation of HgCl in Fe/SV-GN and Fe/SV-N3 is ten times as large as that in Fe/DV-GN and Fe/DV-N4. The direction of electron transfer in Fe/SV-GN and Fe/SV-N3 is from graphene-based substrates and Fe atom to HgCl, while the direction of electron transfer in Fe/DV-GN and Fe/DV-N4 is from graphene-based substrates to Fe atom and HgCl. The different electron transfer mechanism may cause the difference in charge variation of HgCl.

In order to investigate the desorption characteristic of HgCl on Fe/GS, the potential energy diagrams of HgCl on Fe/GS were calculated in Fig. 8. From Fig. 8, in dissociation adsorption model, Hg atom is likely to desorb and convert to  $\text{Hg}^0$ , because only no more than 0.1 eV energy is needed for Hg desorption. In molecule adsorption model, desorption of Cl atom from Fe/GS is difficult to take place for its high energy barrier, so HgCl molecule can be firmly adsorbed on the surface of Fe/GS. According to the exothermic property, dissociation adsorption is more favorable in thermodynamics. Therefore, HgCl molecule inclines to the dissociated adsorption on Fe/GS, which is accordance with the HgCl adsorption on  $\text{Fe}_2\text{O}_3$  [67], ZnO [68] and  $\text{MnFe}_2\text{O}_4$  [69].

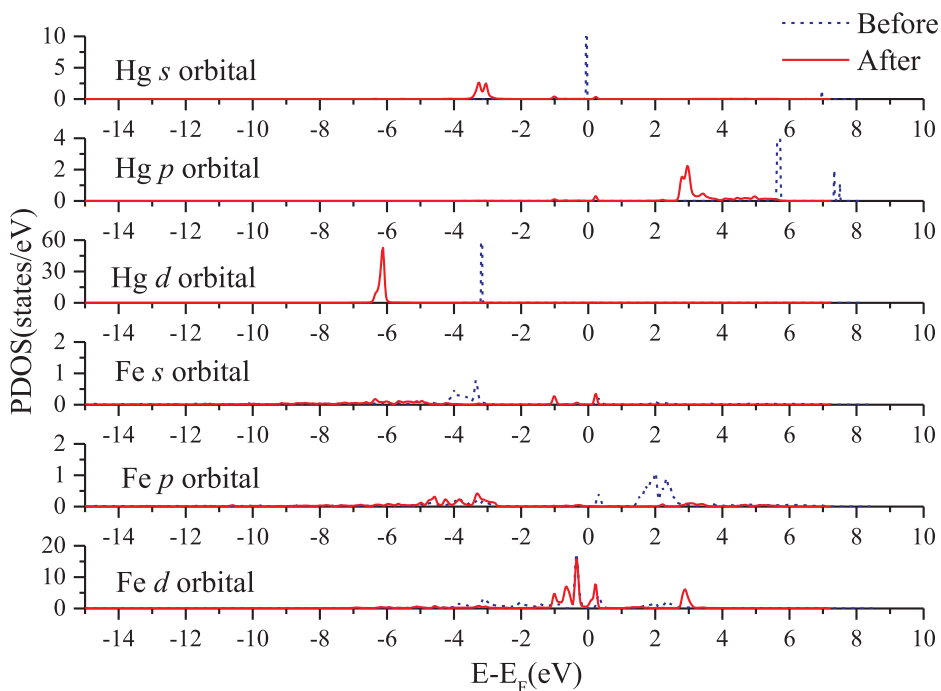


Fig. 6. The projected density of states diagrams of  $\text{Hg}^0$  and Fe atom on Fe/DV-N4.

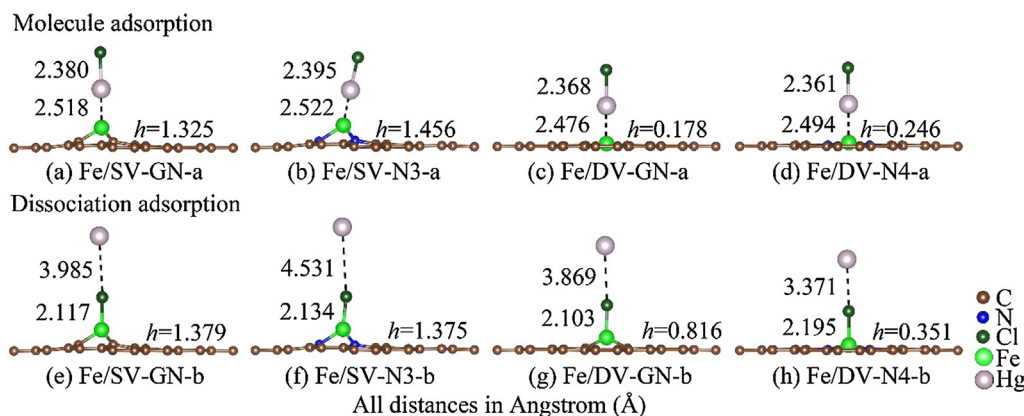


Fig. 7. The adsorption configurations of HgCl on Fe/GS.

Table 3

The uplift height of Fe atom ( $\Delta h$ , Å), charge variation ( $\Delta q$ , e) and adsorption energy ( $E_{\text{ads}}$ , eV) for HgCl adsorption system in molecular adsorption model.

Molecule	$\Delta h$ (Å)	$\Delta q_{\text{HgCl}}$ (e)	$\Delta q_{\text{Fe}}$ (e)	$\Delta q_{\text{sub}}$ (e)	$E_{\text{ads}}$ (eV)
Fe/SV-GN	-0.020	0.312	-0.041	-0.245	-1.866
Fe/SV-N3	0.218	0.386	-0.001	-0.356	-2.126
Fe/DV-GN	-0.336	0.038	0.006	-0.042	-1.749
Fe/DV-N4	0.194	0.085	0.022	-0.107	-1.493

Table 4

The uplift height of Fe atom ( $\Delta h$ , Å), charge variation ( $\Delta q$ , e) and adsorption energy ( $E_{\text{ads}}$ , eV) for HgCl adsorption system in dissociation adsorption model.

Dissociation	$\Delta h$ (Å)	$\Delta q_{\text{HgCl}}$ (e)	$\Delta q_{\text{Fe}}$ (e)	$\Delta q_{\text{sub}}$ (e)	$E_{\text{ads}}$ (eV)
Fe/SV-GN	0.034	0.498	-0.163	-0.321	-2.880
Fe/SV-N3	0.136	0.594	-0.251	-0.332	-3.172
Fe/DV-GN	0.302	0.424	-0.105	-0.304	-2.267
Fe/DV-N4	0.299	0.478	-0.062	-0.397	-1.653

Furthermore, HgCl, an important intermediate for Hg<sup>0</sup> oxidation, cannot adsorb molecularly on Fe/GS, which implies that the oxidation of Hg<sup>0</sup> on Fe/GS may take place in one step oxidation mode, such as the oxidation of Hg<sup>0</sup> on the surface of Au [70].

### 3.2.3. HgCl<sub>2</sub> adsorption

The stable adsorption configurations of HgCl<sub>2</sub> on Fe/GS are shown in Fig. 9, and corresponding key parameters of adsorption process are summarized in Table 5 and Table 6. From Fig. 9, there are two main adsorption model according to the adsorption configurations of HgCl<sub>2</sub> on Fe/GS, vertical adsorption and bending adsorption, and some important bond lengths are marked. In vertical adsorption model, the bond lengths of Hg–Cl are all stretched compared to HgCl<sub>2</sub> molecule (2.31 Å) [66], suggesting that there is a bonding interaction between HgCl<sub>2</sub> molecule and Fe/GS. In detail, the bond length of Hg–Cl on Fe/SV-N3 in vertical adsorption model is longest (3.085 Å), and corresponding adsorption energy is largest (–1.194 eV) at the same time. In bending adsorption model, there are two bonding interaction between HgCl<sub>2</sub> molecule and Fe/GS, and the adsorption energy is bigger than that in vertical adsorption model. From Table 5 and Table 6, there is an obvious difference of HgCl<sub>2</sub> adsorption energy on different Fe/GS, confirming that graphene-based substrates have an important influence on HgCl<sub>2</sub> adsorption on Fe/GS. In detail, the adsorption of HgCl<sub>2</sub> on Fe/GS is unstable because its adsorption energy is positive, while Fe/SV-N3 has the biggest adsorption energy in both adsorption model which suggests that Fe/SV-N3 has high adsorption activity for HgCl<sub>2</sub>.

The potential energy diagrams of HgCl<sub>2</sub> on Fe/GS were calculated to investigate the desorption characteristic of HgCl<sub>2</sub> on Fe/GS. From

Fig. 10, in vertical adsorption model, the adsorbed HgCl<sub>2</sub> molecule will desorb from the surface of Fe/GS in the form of HgCl molecule, because the energies needed are 0.509, 0.412, 0.529 and 0.357 eV respectively, which is relatively easy to take place in coal-fired flue gas environment. Specially, HgCl<sub>2</sub> molecules adsorbed on Fe/DV-GN and Fe/DV-N4 are more likely to desorb from Fe/GS in the form of HgCl<sub>2</sub> molecule, because the energy of 0.416 eV is needed for HgCl<sub>2</sub> desorption on Fe/DV-GN and there is no energy needed for HgCl<sub>2</sub> desorption on Fe/DV-N4. In bending adsorption model, expect for Fe/DV-N4, the adsorbed HgCl<sub>2</sub> molecule can firmly exist on the surface of Fe/GS. Compared with vertical adsorption, the bending adsorption is the main adsorption model according to thermodynamic stability. Noteworthy, in Fig. 10(d), from Fe/DV-N4-Cl + HgCl(g) to Fe/DV-N4-HgCl<sub>2</sub> (h or d), the oxidation of HgCl on the chlorinated surface of Fe/DV-N4 is exothermic reaction which indicates that the oxidation of HgCl is thermodynamically favorable. From Fe/DV-N4-HgCl<sub>2</sub> (h or d) to Fe/DV-N4 + HgCl<sub>2</sub>(g), the formation product (HgCl<sub>2</sub>) cannot be adsorbed firmly on the surface of Fe/DV-N4, indicating that the desorption of HgCl<sub>2</sub> is thermodynamically favorable and can take place spontaneously. Therefore, the oxidation reaction of Hg<sup>0</sup> on the surface Fe/DV-N4 may be promoted through accelerating the oxidation process of HgCl and the HgCl<sub>2</sub> desorption form Fe/DV-N4. The detail oxidation reaction mechanism should be performed in the further to examine whether Fe/DV-N4 can be a promising catalyst for Hg<sup>0</sup> oxidation.

### 3.3. Electronic structure analysis

From the above analysis, the effect of graphene-based substrates on mercury species adsorption is significant, and the difference of adsorption energy between different Fe/GS originates from the effect of graphene-based substrates. Furthermore, it is known that there is a close relationship between performance of catalysts and electric structure of catalysts. In order to gain further insight to the support effects of graphene-based substrates, the analysis of *d*-band center and Fermi softness were performed.

The previous studies have demonstrated that the *d*-band center is a good descriptor of activity of transition-metal surface and it can be calculated from the following equation [64,71]:

$$\varepsilon_d = \frac{\int_{-\infty}^{+\infty} E \cdot D(E) dE}{\int_{-\infty}^{+\infty} D(E) dE} \quad (1)$$

$D(E)$  is the *d* states of Fe atom in Fe/GS. The *d*-band center value of Fe/SV-GS, Fe/SV-N3, Fe/DV-GS and Fe/DV-N4 are –0.97, –1.85, –1.17 and –1.15 eV, respectively. According to the calculated value of *d*-band center, the adsorption activity of four Fe/GS should decrease in the following order, Fe/SV-GN > Fe/DV-N4 > Fe/DV-GN > Fe/SV-N3, while the sequence of adsorption activity of four Fe/GS based on the calculated data of adsorption energy is Fe/SV-N3 > Fe/SV-

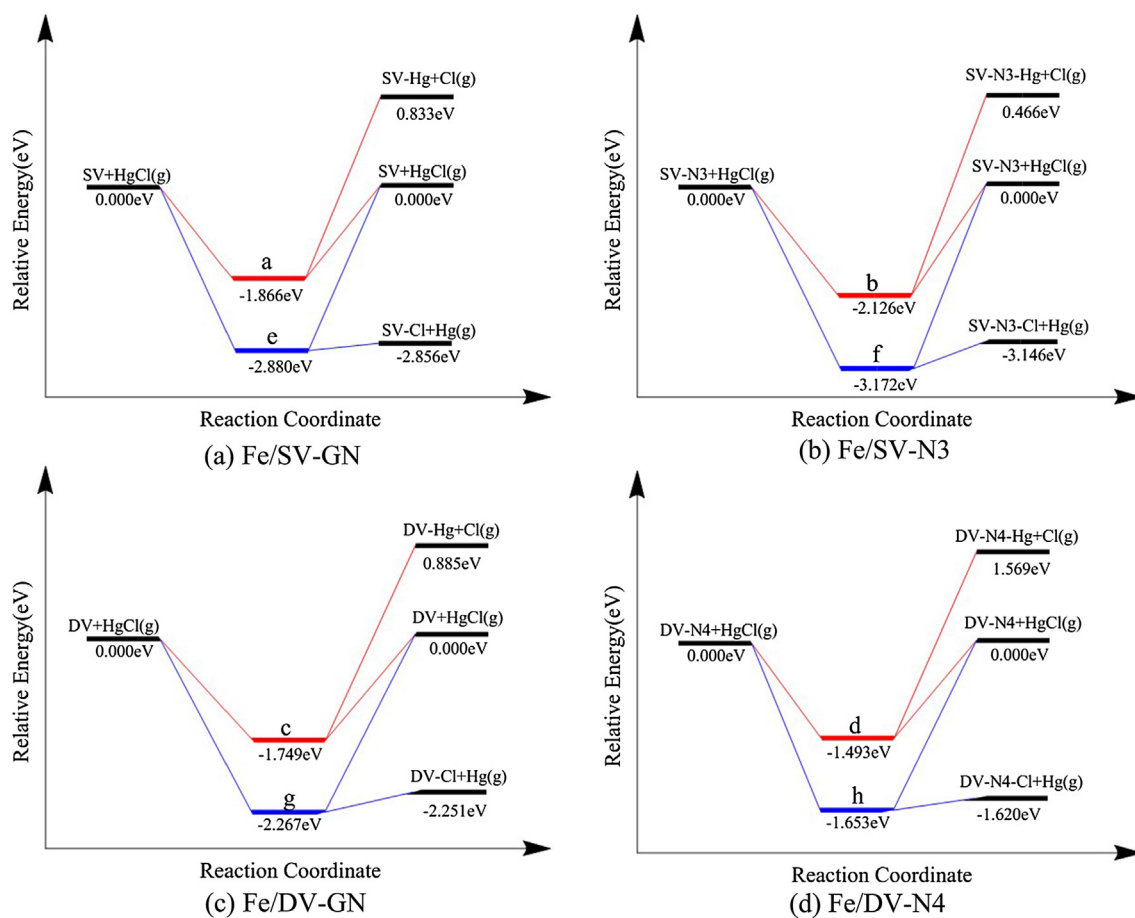


Fig. 8. The potential energy diagrams of HgCl on Fe/GS.

GN > Fe/DV-GN > Fe/DV-N4. The contradictory adsorption activity order suggests that the *d*-band center is not suitable to describe the adsorption activity of Fe/GS.

According to frontier molecular orbital theory, the whole frontier electronic band of the solid surface is reactive. It is known that the closer the electronic state to the Fermi level, the greater the contribution to bonding interaction. Therefore, the reactivity of a catalyst should be determined by both density of states ( $g(E)$ ) and a weight function ( $W(E)$ ) which quantifies the contribution of every electronic state to the surface bonding. According to this idea, Fermi softness ( $S_F$ ), which can describe the chemical reactivity of solid surfaces in quantity, is proposed by the research group of Zhuang [72]. In addition,

Table 5

The uplift height of Fe atom ( $\Delta h$ , Å), charge variation ( $\Delta q$ , e) and adsorption energy ( $E_{ads}$ , eV) for HgCl<sub>2</sub> adsorption system in vertical adsorption model.

Vertical	$\Delta h$ (Å)	$\Delta q_{HgCl_2}$ (e)	$\Delta q_{Fe}$ (e)	$\Delta q_{sub}$ (e)	$E_{ads}$ (eV)
Fe/SV-GN	0.127	0.340	-0.115	-0.204	-0.751
Fe/SV-N3	0.255	0.722	-0.105	-0.604	-1.194
Fe/DV-GN	0.422	0.221	-0.044	-0.156	-0.416
Fe/DV-N4	0.007	0.155	0.034	-0.167	0.387

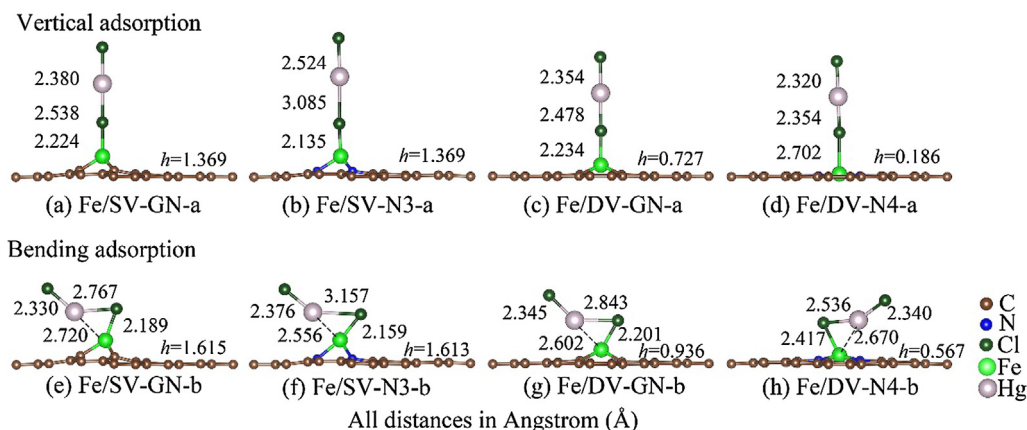


Fig. 9. The adsorption configurations of HgCl<sub>2</sub> on Fe/GS.

**Table 6**  
The uplift height of Fe atom ( $\Delta h$ , Å), charge variation ( $\Delta q$ , e) and adsorption energy ( $E_{\text{ads}}$ , eV) for  $\text{HgCl}_2$  adsorption system in bending adsorption model.

Bending	$\Delta h$ (Å)	$\Delta q_{\text{HgCl}_2}$ (e)	$\Delta q_{\text{Fe}}$ (e)	$\Delta q_{\text{sub}}$ (e)	$E_{\text{ads}}$ (eV)
Fe/SV-GN	0.270	0.299	-0.096	-0.165	-1.010
Fe/SV-N3	0.375	0.652	-0.146	-0.471	-2.234
Fe/DV-GN	0.422	0.361	-0.086	-0.256	-0.801
Fe/DV-N4	0.515	0.298	0.095	-0.354	0.403

according to our previous studies [39], we found that the chemical activity of Fe/GS on toxic gases adsorption can be well described by the Fermi softness ( $S_F$ ). Therefore, we try to understand the difference of adsorption energy between different Fe/GS through  $S_F$ . The  $S_F$  can be calculated from the following equation:

$$S_F = \int_{-\infty}^{+\infty} g(E)W(E)dE \quad (2)$$

where  $g(E)$  is the total density of states.  $W(E)$  is can be acquired from the derivative of the Fermi-Dirac function,  $-f'_T(E-E_F)$ . The  $-f'_T(E-E_F)$  is defined as the following equation:

$$-f'_T(E-E_F) = \frac{1}{k_B T} \frac{1}{(e^{(E-E_F)/k_B T} + 1)(e^{(E_F-E)/k_B T} + 1)} \quad (3)$$

where  $k_B T$  is the nominal electron temperature ( $k$  is the Boltzmann constant and  $T$  is parametric temperature) [72]. According to previous researches [39,72,73], the  $S_F$  is can be adjusted with the value of  $kT$ , and the selection of  $kT$  is depended on adsorbates. For example, the adsorption of H atom on  $\text{VS}_2$  surface [74] and the adsorption of O atom on 27 kinds of Pd derived surfaces [72] can be well characterized by Fermi softness when the value of  $kT$  is 0.4 eV, while the adsorption of

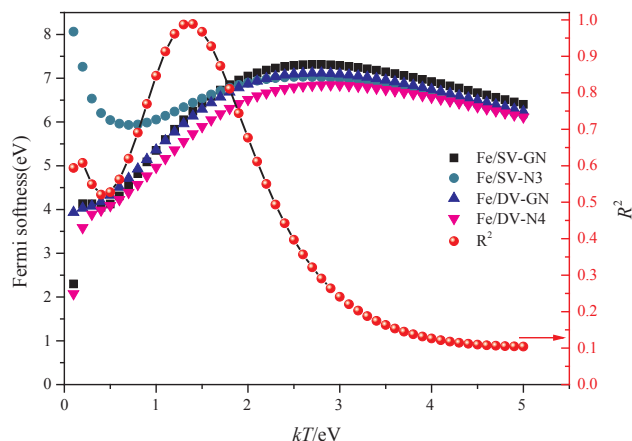


**Fig. 11.** The effect of  $kT$  on Fermi softness and the square of the correlation coefficient.

$\text{NO}_2$ ,  $\text{NH}_3$ ,  $\text{SO}_3$  and  $\text{H}_2\text{S}$  on the surface of single atom iron catalysts with graphene-based substrates can be well characterized by Fermi softness at  $kT = 0.25$  eV. Therefore, we calculated the  $S_F$  of four kinds of Fe/GS with different  $kT$  to investigate the effect of  $kT$  on  $S_F$ , and the square of correlation coefficient ( $R^2$ ) between adsorption energy of  $\text{Hg}^0$  and  $S_F$  with different  $kT$  was plotted to select the optimal value of  $S_F$  for next analysis, as shown in Fig. 11. From Fig. 11, the value of  $S_F$  and  $R^2$  varies with  $kT$ , and  $R^2$  reaches the maximum value (0.99) when  $kT$  is 1.35 eV, and the Fermi softness of Fe/SV-GN, Fe/SV-N3, Fe/DV-GN and Fe/DV-N4 are 6.15, 6.39, 6.05 and 5.64 eV, respectively.

In order to further verify the correlation between  $S_F$  and  $E_{\text{ads}}$ ,

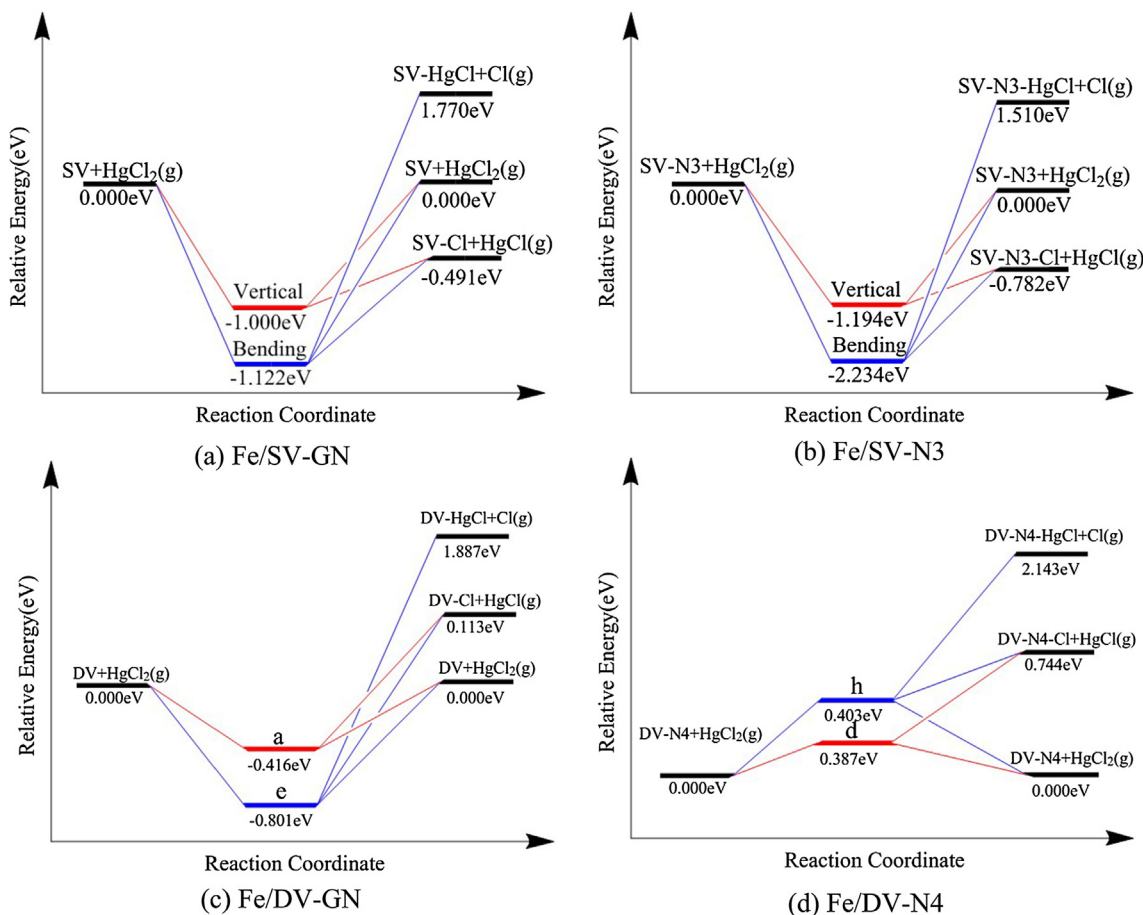


**Fig. 10.** The potential energy diagrams of  $\text{HgCl}_2$  on Fe/GS.

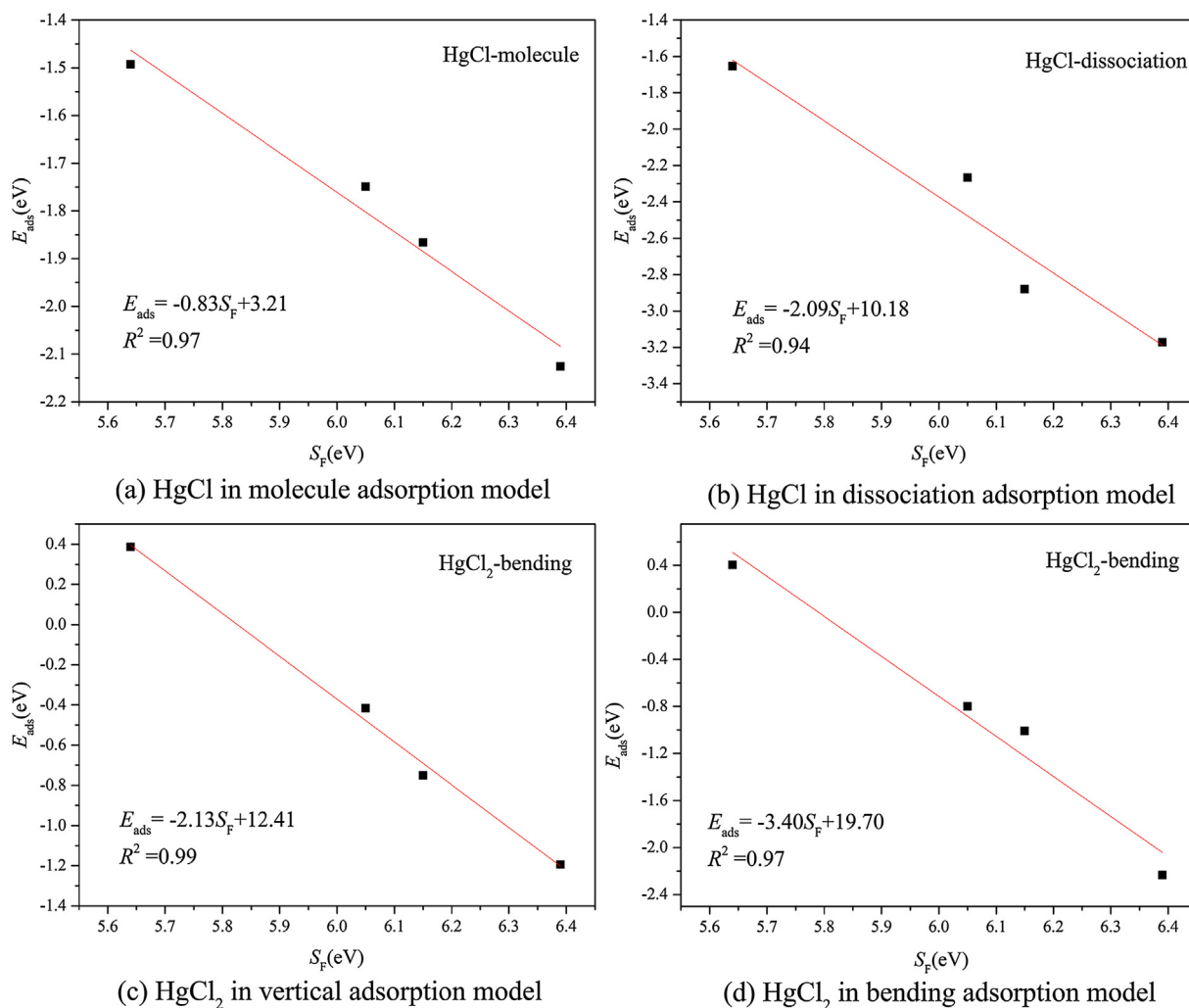


Fig. 12. The adsorption energies of HgCl and HgCl<sub>2</sub> as a function of  $S_F$  ( $kT = 1.35$  eV).

adsorption energies of HgCl and HgCl<sub>2</sub> as a function of  $S_F$  ( $kT = 1.35$  eV) were plotted, as shown in Fig. 12. From Fig. 12, an obvious relationship between adsorption energy and Fermi softness can be found. The  $R^2$  between adsorption energy and Fermi softness for HgCl and HgCl<sub>2</sub> all exceed 0.9, confirming that Fermi softness is an efficient descriptor for adsorption activity of the present adsorption system. Furthermore, we can apply Fermi softness as indicator to design new graphene-based single atom catalysts.

### 3.4. Thermodynamic analysis

From adsorption and electronic structure analysis, the support effects of graphene-based substrates have been well understood, and the effect of temperature of adsorption energy should be further considered for practical application. Therefore, the thermodynamic analysis was performed through Gibbs free energy calculation under different temperature. The Gibbs free energy of gas and solid can be calculated from the following equations [62,63,75,76]:

$$G_{\text{gas}} = E_{\text{ele}} + ZPE + RT - TS \quad (4)$$

$$G_{\text{solid}} = E_{\text{ele}} + ZPE - TS \quad (5)$$

where  $E_{\text{ele}}$  is the ground-state energy of the system; ZPE is the zero correction energy; R is gas constant; T is the temperature; S is the entropy; ZPE and S can also be obtained through frequency calculation. Furthermore, Gibbs free energy was applied to redefine the adsorption energy through the following equation:

$$\Delta G = G_{\text{Hg-Fe/GS}} - G_{\text{Fe/GS}} - G_{\text{Hg}} \quad (6)$$

where  $G_{\text{Hg-Fe/GS}}$ ,  $G_{\text{Fe/GS}}$  and  $G_{\text{Hg}}$  are the Gibbs free energy of adsorption systems, Fe/GS and mercury species, respectively. From this calculation formula, a negative value of  $\Delta G$  suggests adsorption process can take place spontaneously and a higher negative value of  $\Delta G$  corresponds to a stronger adsorption interaction. According to the coal-fired power plant operation conditions, we select a wide temperature range (298.15–1000 K) to calculate the  $\Delta G$  of mercury species on different Fe/GS, as shown in Fig. 13.

From Fig. 13, the value of  $\Delta G$  increases with the increase of temperature, indicating that low temperature accelerates mercury species removal. In detail, the adsorption process of Hg<sup>0</sup>, HgCl (molecule and dissociation adsorption model) and HgCl<sub>2</sub> (bending adsorption model) can take place spontaneously at the selected temperature range (298.15 K to 1000 K) for its negative value of  $\Delta G$ , suggesting that Fe/SV-N3 has super high adsorption activity for mercury species. However, according to above potential energy diagrams of HgCl and HgCl<sub>2</sub> (Fig. 8(b) and Fig. 10(b)), the decomposition of adsorbed HgCl and HgCl<sub>2</sub> can take place on the surface of Fe/SV-N3 which indicates that Fe/SV-N3 cannot firmly adsorb HgCl and HgCl<sub>2</sub>. Therefore, considering the adsorption and desorption properties of mercury species, it may be suitable for Fe/SV-N3 to be a new adsorbent for removing Hg<sup>0</sup> pollutant. Different from Fe/SV-N3, the value of  $\Delta G$  for Hg<sup>0</sup> and HgCl<sub>2</sub> on Fe/DV-N4 are all positive, which suggests that Fe/DV-N4 has the lowest affinity for Hg<sup>0</sup> and HgCl<sub>2</sub>. From the obvious difference between Fe/SV-N3 and Fe/DV-N4 in mercury species adsorption, the support effects of

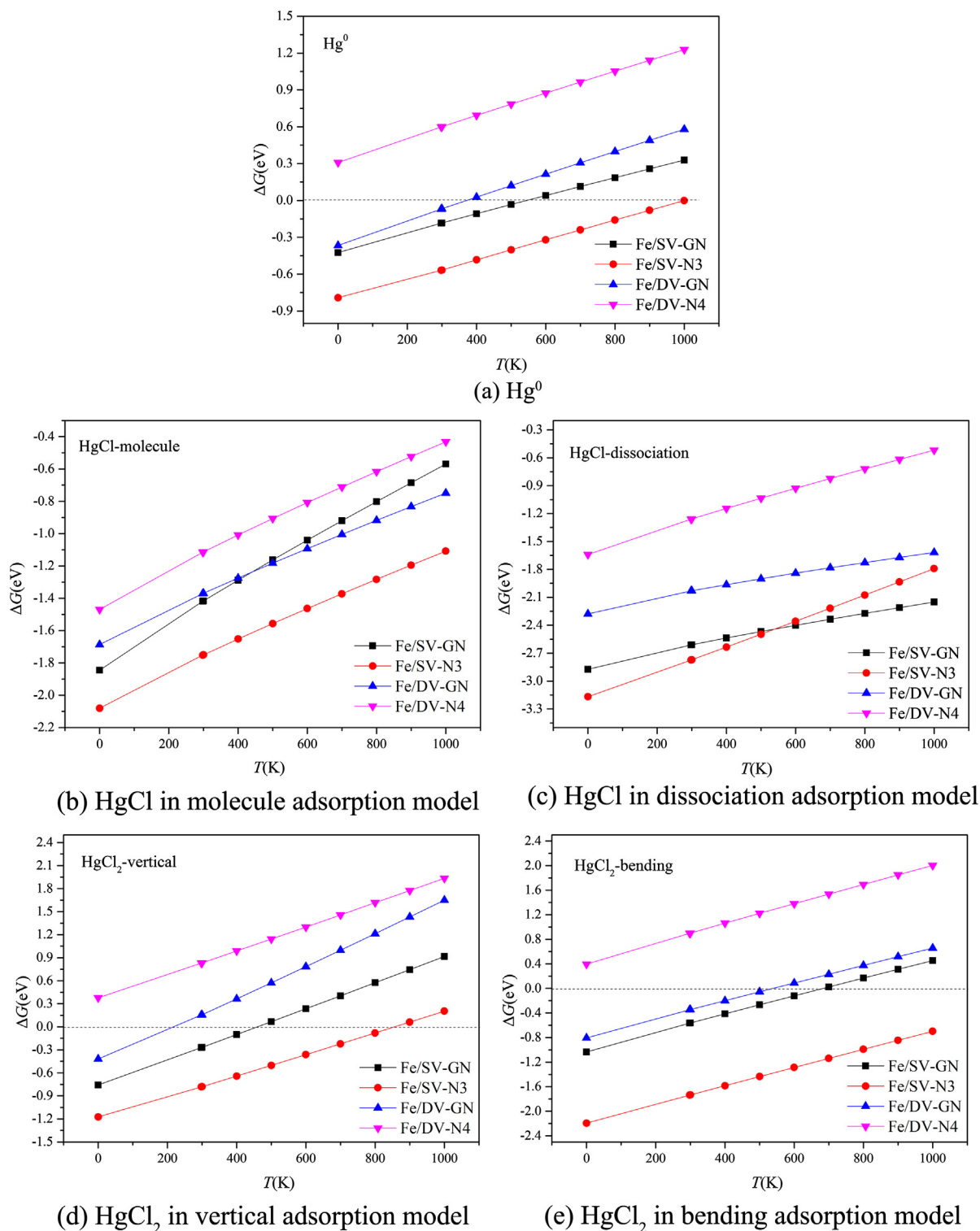


Fig. 13. The  $\Delta G$  of mercury species on different Fe/GS as a function of temperature.

graphene-based substrates on the properties of SACs can be proved again.

#### 4. Conclusion

The adsorption characteristics of mercury species on four kinds of Fe/GS were systematically investigated through the adsorption configurations, projected density of states, potential energy diagrams, electronic structure and thermodynamic analysis. It is found that the

support effect of graphene-based substrates on mercury species adsorption is significant, and we can design new graphene-based materials with different properties through modifying graphene-based substrates. According to the adsorption characteristic and thermodynamic analysis, it is reasonable that Fe/SV-N3 can be used as a new adsorbent for removing  $Hg^0$ .

Moreover,  $d$  band center is not suitable for describe the adsorption activity of Fe/GS, while Fermi softness is a good descriptor for adsorption activity of Fe/GS. Fermi softness can not only be a bridge

between support effects and electronic structure, but also be utilized to design and optimization of new catalysts. We hope this work can provide a novel perspective for adsorption and oxidation of Hg and lay a foundation for the further study of graphene-based support effects in single atom catalysts.

For further investigations, the adsorption characteristics of HCl, Cl<sub>2</sub> and O<sub>2</sub> on the surface of Fe/GS will be researched to lay a foundation for studying catalytic oxidation of Hg<sup>0</sup>. The catalytic oxidation of Hg<sup>0</sup> on Fe/GS will be studied to further confirm the catalytic activity of Fe/GS, and the support effects of graphene-based substrates on energy barrier will also be discussed for catalyst optimization. Additionally, according to diversity and complexity of flue gas, such as SO<sub>2</sub> and H<sub>2</sub>O, the effects of flue gas on catalytic oxidation will also be studied.

## Acknowledgement

This work was supported by the National Natural Science Foundation of China (No. 91545122), Beijing Natural Science Foundation (2182066), Natural Science Foundation of Hebei Province of China (B2018502067) and the Fundamental Research Funds for the Central Universities (JB2015RCY03 and 2017XS121). Computational resources from the Lvliang Supercomputer Center were acknowledged.

## Appendix A. Supplementary material

Supplementary data associated with this article can be found, in the online version, at <https://doi.org/10.1016/j.apsusc.2018.06.031>.

## References

- T.D. Brown, D.N. Smith, R.A. Hargis, W.J. O'Dowd, Mercury measurement and its control: what we know, have learned, and need to further investigate, *J. Air Waste Manage. Assoc.* 49 (6) (1999) 1–97.
- Y. Gao, Z. Li, A DFT study of the Hg<sup>0</sup> oxidation mechanism on the V<sub>2</sub>O<sub>5</sub>-TiO<sub>2</sub>(001) surface, *Mol. Catal.* 433 (2017) 372–382.
- Y. Tan, R. Mortazavi, B. Dureau, M.A. Douglas, An investigation of mercury distribution and speciation during coal combustion, *Fuel* 83 (16) (2004) 2229–2236.
- Y. Cao, B. Chen, J. Wu, H. Cui, J. Smith, C.K. Chen, P. Chu, W.P. Pan, Study of mercury oxidation by a selective catalytic reduction catalyst in a pilot-scale slip-stream reactor at a utility boiler burning bituminous coal, *Energy Fuels* 21 (1) (2007) 145–156.
- L. Tong, T. Yue, P. Zuo, X.X. Zhang, C.L. Wang, J.J. Gao, K. Wang, Effect of characteristics of KI-impregnated activated carbon and flue gas components on Hg<sup>0</sup> removal, *Fuel* 197 (2017) 1–7.
- C. Zhu, Y. Duan, C.-Y. Wu, Q. Zhuo, M. She, T. Yao, J. Zhang, Mercury removal and synergistic capture of SO<sub>2</sub>/NO by ammonium halides modified rice husk char, *Fuel* 172 (2016) 160–169.
- H. Yi, Y. Zuo, H. Liu, X.L. Tang, S.Z. Zhao, Z.X. Wang, F.Y. Gao, B.W. Zhang, Simultaneous removal of SO<sub>2</sub>, NO, and CO<sub>2</sub> on metal-modified coconut shell activated carbon, *Water, Air Soil Pollut.* 225 (5) (2014).
- D.H. Lim, S. Aboud, J. Wilcox, Investigation of adsorption behavior of mercury on Au(111) from first principles, *Environ. Sci. Technol.* 46 (13) (2012) 7260–7266.
- Y. Zhao, M.D. Mann, J.H. Pavlish, B.A. Mibeck, G.E. Dunham, E.S. Olson, Application of gold catalyst for mercury oxidation by chlorine, *Environ. Sci. Technol.* 40 (5) (2006) 1603–1608.
- J.-E. Jung, D. Geatches, K. Lee, S. Aboud, G.E. Brown Jr, J. Wilcox, First-principles investigation of mercury adsorption on the  $\alpha$ -Fe<sub>2</sub>O<sub>3</sub>(1102) surface, *J. Phys. Chem. C* 119 (47) (2015) 26512–26518.
- S. Sun, D. Zhang, C. Li, Y.J. Wang, Q.S. Yang, Density functional theory study of mercury adsorption and oxidation on CuO(111) surface, *Chem. Eng. J.* 258 (2014) 128–135.
- G. Xin, P. Zhao, C. Zheng, Theoretical study of different speciation of mercury adsorption on CaO (001) surface, *Proc. Combust. Inst.* 32 (2) (2009) 2693–2699.
- J. Zhao, M.-C. He, Theoretical study of heavy metal Cd, Cu, Hg, and Ni(II) adsorption on the kaolinite(001) surface, *Appl. Surf. Sci.* 317 (2014) 718–723.
- Y. Liu, H. Li, J. Liu, Theoretical prediction the removal of mercury from flue gas by MOFs, *Fuel* 184 (2016) 474–480.
- L. Zhao, C. Li, X. Zhang, G.M. Zeng, J. Zhang, Y.N. Xie, A review on oxidation of elemental mercury from coal-fired flue gas with selective catalytic reduction catalysts, *Catal. Sci. Technol.* 5 (7) (2015) 3459–3472.
- L. Wang, H. Li, W. Zhang, X. Zhao, J.X. Qiu, A.W. Li, X.S. Zheng, Z.P. Hu, R. Si, J. Zeng, Supported rhodium catalysts for ammonia-borane hydrolysis: dependence of the catalytic activity on the highest occupied state of the single rhodium atoms, *Angew. Chem.* 56 (17) (2017) 4712–4718.
- E.J. Peterson, A.T. DeLaRiva, S. Lin, R.S. Johnson, H. Guo, J.T. Miller, J.H. Kwak, C.H. Peden, B. Kiefer, L.F. Allard, F.H. Ribeiro, A.K. Datye, Low-temperature carbon monoxide oxidation catalysed by regenerable atomically dispersed palladium on alumina, *Nat. Commun.* 5 (2014) 4885.
- J. Lin, A. Wang, B. Qiao, X.Y. Liu, X.F. Yang, X.D. Wang, J.X. Liang, J. Li, J.Y. Liu, T. Zhang, Remarkable performance of Ir<sub>1</sub>/FeO<sub>x</sub> single-atom catalyst in water gas shift reaction, *J. Am. Chem. Soc.* 135 (41) (2013) 15314–15317.
- C.T. Wu, K.M. Yu, F. Liao, N. Young, P. Nellist, A. Dent, A. Kroner, S.C.E. Tsang, A non-syn-gas catalytic route to methanol production, *Nat. Commun.* 3 (2012) 1050.
- B. Qiao, A. Wang, X. Yang, L.F. Allard, Z. Jiang, Y.T. Cui, J.Y. Liu, Li Jun, Single-atom catalysis of CO oxidation using Pt<sub>1</sub>/FeO<sub>x</sub>, *Nat. Commun.* 3 (8) (2011) 634–641.
- B.F. Machado, P. Serp, Graphene-based materials for catalysis, *Catal. Sci. Technol.* 2 (1) (2012) 54–75.
- G. Xu, R. Wang, F. Yang, D.W. Ma, Z.X. Yang, Z.S. Lu, CO oxidation on single Pd atom embedded defect-graphene via a new termolecular Eley-Rideal mechanism, *Carbon* 118 (2017) 35–42.
- Y. Tang, J. Zhou, Z. Shen, W.G. Chen, C.G. Li, X.Q. Dai, High catalytic activity for CO oxidation on single Fe atom stabilized in graphene vacancies, *RSC Adv.* 6 (96) (2016) 93985–93996.
- L. Wang, Q. Luo, W. Zhang, J.L. Yang, Transition metal atom embedded graphene for capturing CO: a first-principles study, *Int. J. Hydrogen Energy* 39 (35) (2014) 20190–20196.
- S.G. Liu, S.P. Huang, Theoretical insights into the activation of O<sub>2</sub> by Pt single atom and Pt<sub>4</sub> nanocluster on functionalized graphene support: critical role of Pt positive polarized charges, *Carbon* 115 (2017) 11–17.
- T. Zhang, Q. Xue, M. Shan, Z.Y. Jiao, X.Y. Zhou, C.C. Ling, Z.F. Yan, Adsorption and catalytic activation of O<sub>2</sub> molecule on the surface of au-doped graphene under an external electric field, *J. Phys. Chem. C* 116 (37) (2012) 19918–19924.
- X. Li, W. Bi, M. Chen, Y.X. Sun, H.X. Ju, W.S. Yan, J.F. Zhu, X.J. Wu, W.S. Chu, C.Z. Wu, Y. Xie, Exclusive Ni-N4 sites realize near-unity CO selectivity for electrochemical CO<sub>2</sub> reduction, *J. Am. Chem. Soc.* 139 (42) (2017) 14889–14892.
- X. Li, W. Bi, L. Zhang, S. Tao, W.S. Chu, Q. Zhang, Y. Luo, C.Z. Wu, Y. Xie, Single-atom Pt as co-catalyst for enhanced photocatalytic H<sub>2</sub> evolution, *Adv. Mater.* 28 (12) (2016) 2427–2431.
- Y. Chen, S. Ji, Y. Wang, Q.C. Dong, W.X. Chen, Z. Li, R.G. Shen, L.R. Zheng, Z.B. Zhuang, D.S. Wang, Y.D. Li, Isolated single iron atoms anchored on N-doped porous carbon as an efficient electrocatalyst for the oxygen reduction reaction, *Angew. Chem.* 129 (24) (2017) 7041–7045.
- X. Chen, L. Yu, S. Wang, D.H. Deng, X.H. Bao, Highly active and stable single iron site confined in graphene nanosheets for oxygen reduction reaction, *Nano Energy* 32 (2017) 353–358.
- Y. Fan, Y. Zhuo, Z. Zhu, L.L. Li, Q. Chen, Y. Lou, Density functional theory study on Hg removal mechanisms of Cu-impregnated activated carbon prepared by simplified method, *Korean J. Chem. Eng.* 33 (10) (2016) 2869–2877.
- L. Fan, L. Ling, B. Wang, R.G. Zhang, The adsorption of mercury species and catalytic oxidation of Hg<sup>0</sup> on the metal-loaded activated carbon, *Appl. Catal. A* 520 (2016) 13–23.
- M.T. Izquierdo, D. Ballester, R. Juan, G.D. Enrique, B. Rubio, C. Ruiz, M.R. Pino, Tail-end Hg capture on Au/carbon-monolith regenerable sorbents, *J. Hazard. Mater.* 193 (2011) 304–310.
- Y. Liu, Elemental Mercury Removal from Flue Gas by Metal/Metal Oxide Decorated Graphene Oxide Composites, University of Alberta, Edmonton, 2014.
- Y. Tang, S. Zhao, B. Long, J.C. Liu, J. Li, On the nature of support effects of metal dioxides MO<sub>2</sub>(M = Ti, Zr, Hf, Ce, Th) in single-atom gold catalysts: importance of quantum primogenic effect, *J. Phys. Chem. C* 120 (31) (2016) 17514–17526.
- S. Yang, Y.J. Tak, J. Kim, A. Soon, H. Lee, Support effects in single-atom platinum catalysts for electrochemical oxygen reduction, *ACS Catal.* 7 (2) (2017) 1301–1307.
- Y. Lou, J. Liu, CO oxidation on metal oxide supported single Pt atoms: the role of the support, *Ind. Eng. Chem. Res.* 56 (24) (2017) 6916–6925.
- C.S. Ewing, A. Bagussety, E.G. Patriarca, D.S. Lambrecht, G. Vesper, J.K. Johnson, Impact of support interactions for single-atom molybdenum catalysts on amorphous silica, *Ind. Eng. Chem. Res.* 55 (48) (2016) 12350–12357.
- Z. Gao, W. Yang, X. Ding, G. Lv, W.P. Yan, Support effects in single atom iron catalysts on adsorption characteristics of toxic gases (NO<sub>2</sub>, NH<sub>3</sub>, SO<sub>3</sub> and H<sub>2</sub>S), *Appl. Surf. Sci.* 436 (2018) 585–595.
- G. Kresse, D. Joubert, From ultrasoft pseudopotentials to the projector augmented-wave method, *Phys. Rev. B* 59 (3) (1999) 1758.
- G. Kresse, J. Furthmüller, Efficiency of ab-initio total energy calculations for metals and semiconductors using a plane-wave basis set, *Comput. Mater. Sci.* 6 (1) (1996) 15–50.
- G. Kresse, J. Furthmüller, Efficient iterative schemes for ab initio total-energy calculations using a plane-wave basis set, *Phys. Rev. B* 54 (16) (1996) 11169.
- J.P. Perdew, K. Burke, M. Ernzerhof, Generalized gradient approximation made simple, *Phys. Rev. Lett.* 77 (18) (1996) 3865.
- A.D. Becke, E.R. Johnson, Exchange-hole dipole moment and the dispersion interaction, *J. Chem. Phys.* 122 (15) (2005) 154104.
- J. Liu, M.A. Cheney, F. Wu, M. Li, Effects of chemical functional groups on elemental mercury adsorption on carbonaceous surfaces, *J. Hazard. Mater.* 186 (1) (2011) 108–113.
- W. Xiang, J. Liu, M. Chang, C.G. Zheng, The adsorption mechanism of elemental mercury on CuO (110) surface, *Chem. Eng. J.* 200–202 (2012) 91–96.
- S. Grimme, S. Ehrlich, L. Goerigk, Effect of the damping function in dispersion corrected density functional theory, *J. Comput. Chem.* 32 (7) (2011) 1456–1465.
- S. Grimme, J. Antony, S. Ehrlich, H. Krieg, A consistent and accurate ab initio parametrization of density functional dispersion correction (DFT-D) for the 94 elements H-Pu, *J. Chem. Phys.* 132 (15) (2010) 154104.
- Y. Tang, W. Chen, C. Li, L.J. Pan, X.Q. Dai, D.W. Ma, Adsorption behavior of Co

- anchored on graphene sheets toward NO, SO<sub>2</sub>, NH<sub>3</sub>, CO and HCN molecules, *Appl. Surf. Sci.* 342 (2015) 191–199.
- [50] Y. Lee, S. Lee, Y. Hwang, Y.C. Chung, Modulating magnetic characteristics of Pt embedded graphene by gas adsorption (N<sub>2</sub>, O<sub>2</sub>, NO<sub>2</sub>, SO<sub>2</sub>), *Appl. Surf. Sci.* 289 (2014) 445–449.
- [51] M. Sun, W. Tang, Q. Ren, S. Wang, J. Yu, Y.H. Du, Y.J. Zhang, First-principles study of the alkali earth metal atoms adsorption on graphene, *Appl. Surf. Sci.* 356 (2015) 668–673.
- [52] L. Ma, J.-M. Zhang, K.-W. Xu, V. Ji, A first-principles study on gas sensing properties of graphene and Pd-doped graphene, *Appl. Surf. Sci.* 343 (2015) 121–127.
- [53] K.T. Chan, J.B. Neaton, M.L. Cohen, First-principles study of metal adatom adsorption on graphene, *Phys. Rev. B* 77 (23) (2008).
- [54] C. Riplinger, E.A. Carter, Cooperative effects in water binding to cuprous oxide surfaces, *J. Phys. Chem. C* 119 (17) (2015) 9311–9323.
- [55] W. Tang, E. Sanville, G. Henkelman, A grid-based bader analysis algorithm without lattice bias, *J. Phys.: Condens. Matter* 21 (8) (2009) 084204.
- [56] P. Janthon, S.M. Kozlov, F. Vines, J. Limtrakul, F. Illas, Establishing the accuracy of broadly used density functionals in describing bulk properties of transition metals, *J. Chem. Theory Comput.* 9 (3) (2013) 1631–1640.
- [57] A.V. Krashennnikov, P.O. Lehtinen, A.S. Foster, P. Pyykkö, R.N. Nieminen, Embedding transition-metal atoms in graphene: structure, bonding, and magnetism, *Phys. Rev. Lett.* 102 (12) (2009) 126807.
- [58] A.T. Lee, J. Kang, S.-H. Wei, K.J. Chang, Y.H. Kim, Carrier-mediated long-range ferromagnetism in electron-doped Fe-C4 and Fe-N4 incorporated graphene, *Phys. Rev. B* 86 (16) (2012) 165403.
- [59] S. Kattel, P. Atanassov, B. Kiefer, Stability, electronic and magnetic properties of in-plane defects in graphene: a first-principles study, *J. Phys. Chem. C* 116 (14) (2012) 8161–8166.
- [60] Z. Liu, Y. Zhang, B. Wang, H. Chen, X.R. Cheng, Z.C. Huang, DFT study on Al-doped defective graphene towards adsorption of elemental mercury, *Appl. Surf. Sci.* 427 (2018) 547–553.
- [61] D. Cortés-Arriagada, N. Villegas-Escobar, D.E. Ortega, Fe-doped graphene nanosheet as an adsorption platform of harmful gas molecules (CO, CO<sub>2</sub>, SO<sub>2</sub> and H<sub>2</sub>S), and the co-adsorption in O<sub>2</sub> environments, *Appl. Surf. Sci.* 427 (2018) 227–236.
- [62] P. Blowers, B.G. Kim, The adsorption of mercury-species on relaxed and rumbled CaO (001) surfaces investigated by density functional theory, *J. Mol. Model.* 17 (3) (2011) 505–514.
- [63] B. Zhang, J. Liu, C. Zheng, M. Chang, Theoretical study of mercury species adsorption mechanism on MnO<sub>2</sub>(110) surface, *Chem. Eng. J.* 256 (2014) 93–100.
- [64] B. Hammer, J.K. Nørskov, Theoretical surface science and catalysis—calculations and concepts, in: *Adv. Catal.*, vol. 45, Academic Press, 2000, pp. 71–129.
- [65] K. Fukui, Role of frontier orbitals in chemical reactions, *Science* 218 (4574) (1982) 747–754.
- [66] J. Liu, W. Qu, J. Yuan, S.C. Wang, J.R. Qiu, C.G. Zheng, Theoretical studies of properties and reactions involving mercury species present in combustion flue gases, *Energy Fuels* 24 (1) (2010) 117–122.
- [67] P. Guo, X. Guo, C.G. Zheng, Computational insights into interactions between Hg species and  $\alpha$ -Fe<sub>2</sub>O<sub>3</sub>(001), *Fuel* 90 (5) (2011) 1840–1846.
- [68] L. Ling, S. Zhao, P. Han, B.J. Wang, R.X. Zhang, M.H. Fan, Toward predicting the mercury removal by chlorine on the ZnO surface, *Chem. Eng. J.* 244 (2014) 364–371.
- [69] Y. Yang, J. Liu, B. Zhang, Liu Feng, Density functional theory study on the heterogeneous reaction between Hg<sup>0</sup> and HCl over spinel-type MnFe<sub>2</sub>O<sub>4</sub>, *Chem. Eng. J.* 308 (2017) 897–903.
- [70] D.H. Lim, J. Wilcox, Heterogeneous mercury oxidation on au(111) from first principles, *Environ. Sci. Technol.* 47 (15) (2013) 8515–8522.
- [71] J.K. Nørskov, F. Abild-Pedersen, F. Studt, T. Bligaard, Density functional theory in surface chemistry and catalysis, *Proc. Natl. Acad. Sci.* 108 (3) (2011) 937–943.
- [72] B. Huang, L. Xiao, J. Lu, L. Zhuang, Spatially resolved quantification of the surface reactivity of solid catalysts, *Angew. Chem.* 55 (21) (2016) 6239–6243.
- [73] Y. Zhang, X.S. Chen, Y. Huang, C. Zhang, F. Li, H.B. Shu, The role of intrinsic defects in electrocatalytic activity of monolayer VS<sub>2</sub> basal planes for the hydrogen evolution reaction, *J. Phys. Chem. C* 121 (3) (2017) 1530–1536.
- [74] J. Zhu, H. Zhang, Y. Tong, L. Zhao, Y.F. Zhang, Y.Z. Qiu, X.N. Lin, First-principles investigations of metal (V, Nb, Ta)-doped monolayer MoS<sub>2</sub>: Structural stability, electronic properties and adsorption of gas molecules, *Appl. Surf. Sci.* 419 (2017) 522–530.
- [75] D. Loffreda, Theoretical insight of adsorption thermodynamics of multifunctional molecules on metal surfaces, *Surf. Sci.* 600 (10) (2006) 2103–2112.
- [76] W. Ji, Z. Shen, M. Fan, P.R. Su, Q.L. Tang, C.Y. Zou, Adsorption mechanism of elemental mercury (Hg<sup>0</sup>) on the surface of MnCl<sub>2</sub> (110) studied by density functional theory, *Chem. Eng. J.* 283 (2016) 58–64.